

EPJ E

Soft Matter and
Biological Physics

EPJ.org
your physics journal

Eur. Phys. J. E (2011) **34**: 78

DOI: 10.1140/epje/i2011-11078-7

Droplet breakup in an asymmetric microfluidic T junction

Ahmad Bedram and Ali Moosavi



Società
Italiana
di Fisica



Droplet breakup in an asymmetric microfluidic T junction

Ahmad Bedram^a and Ali Moosavi^b

School of Mechanical Engineering, Sharif University of Technology, Azadi Avenue, PO Box 11365-9567 Tehran, Iran

Received 26 January 2011 and Received in final form 19 May 2011

Published online: 8 August 2011 – © EDP Sciences / Società Italiana di Fisica / Springer-Verlag 2011

Abstract. Breakup of non-uniform droplets in an asymmetric T junction consisting of an inlet channel and two different-size outlet channels has been investigated numerically. Also, an analytical approach in the limit of the lubrication approximation has been extended to provide some analytical relations to study the system and verify the numerical results. Parameters that are important in the performance of the system have been determined and discussed. Our results indicate that smaller droplets can be produced by increasing the capillary number. As the geometry becomes symmetric the pressure drop decreases. Our results also reveal that the breakup time and the pressure drop for this system are smaller than the previous suggested method for producing non-uniform droplets, *i.e.*, a uniform size T junction with different-length outlet channels.

1 Introduction

The interest in droplet based microfluidic systems has been increased significantly over the past decade. In these systems, processes such as the transport, mixing, storage and others are performed in separate volumes of the main fluid [1–14]. Not only do these systems prevent contamination and dispersion of the samples, but also they provide better mixing and allow one to conveniently handle minute amounts of liquids in a specific time and speed [2, 5, 13].

In order to use these systems optimally efficient methods should be available to produce a large number of microdroplets in a short time. There exist a variety of methods that allow one to produce microdroplets [1, 3, 4, 6, 8]. However, in most of these methods the produced droplets are either uniform or their sizes are not precisely controlled [15]. In many applications, for example in making emulsions in chemical and pharmaceutical industry, it is necessary to have efficient methods that are capable of producing different droplets with precisely known sizes [8, 16, 17]. In ref. [8] using pressure-driven flow in simple microfluidic configurations two methods for this purpose have been introduced. One of these methods relies on considering an obstacle in the channel containing the droplets. A problem associated with this method is that the produced small and large droplets move together along the channel after the obstacle and a different method is required to separate the droplets. The second method consists of a T junction with side channels that have equal cross-section but the length of the channels is different. The volume ratio of the produced droplets

depends inversely on the length ratio of the channels, namely, $V_1/V_2 \approx \ell_2/\ell_1$, where V_i and ℓ_i ($i = 1, 2$) are the volume of the droplet and the channel length in the outlet channel i , respectively. In this method the size of the system rapidly increases when the volume ratio is large. For example consider a case with $V_1/V_2 = 9$. Since the cross-section areas of the side channels are equal, the length of one of the channels should be almost nine times that of the other. Using asymmetric junctions with different cross-section channels provides another option that has been recently used for producing double-size droplets [16]. However, there is no systematic study on the effects of parameters involved in the system in order to use the method efficiently.

In the present study a Volume of Fluid (VOF) numerical method has been used to investigate the generation of non-uniform droplets in the T junction with different cross-section channels. In order to verify the numerical results an analytical method is extended in the limit of very small contact angles and the numerical results have been compared with the analytical results. Also the results of the investigation have been compared with the results of refs. [13, 14].

2 The system specification

Figure 1 shows the considered system to produce non-uniform droplets. The geometry consists of a T junction with an inlet channel and two different-size outlet channels. In this method an initial droplet (which is suspended in the carrier fluid) enters the T junction through the inlet channel and after reaching the junction breaks up into two

^a e-mail: a_bedram@yahoo.com

^b e-mail: moosavi@sharif.edu

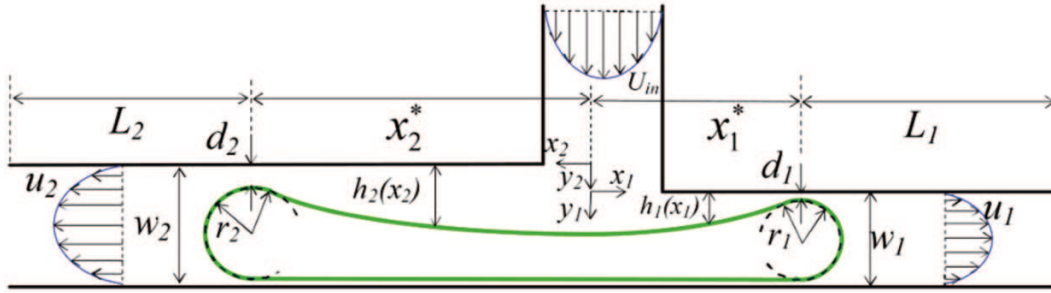


Fig. 1. The geometry of the system considered for producing non-uniform droplets.

unequal parts because of the asymmetry associated with the system. In fig. 1 x and y are the horizontal and vertical components of the coordinate system and subscripts 1 and 2 stand for the flow in the right and the left outlet channels, respectively. U and u represents the average velocity of the carrier fluid in the inlet and outlet channels, respectively. $h(x, y)$ is the thickness of the thin film created between the droplet and the top wall. x^* is the place of minimum thickness and d represents the thickness at x^* . w is the width of the channel and r stands for the radius of curvature of the end parts of the droplet.

3 Analytical solution

It has been recently shown that the behavior of droplets at symmetric T junctions can be classified into three regimes, depending on the flow conditions, size of the droplets and width of the channels, namely, 1) no breakup 2) breakup with tunnel 3) breakup with obstruction [13, 18, 19]. Our numerical results indicate that droplets at asymmetric T junctions may also exhibit all these three regimes.

The analytical analysis reported in this section is an extension of the method for symmetric T junctions [13] and similar to the symmetric case considers only the boundary region between regions of no breakup and breakup with tunnel. In this situation the assumptions made are those pointed out in ref. [13], namely, the capillary number is small and it is also assumed that the pressure drop of the carrier fluid mainly occurs in the thin film between the top wall and the droplet. The final results of this analysis are relations for the smallest thickness of the thin film (d) as a function of other parameters in the outlet channels (see appendix A). These relations are given as

$$\frac{3Ca}{\left[\left(\frac{w_2}{w_1} \right)^2 \left(\frac{\tau_2}{\tau_1} \right)^{5/2} + 1 \right] \left[\frac{w_1}{w_{in}} \right]} = \frac{\tau_1^{5/2}}{\left[\frac{7(1-\tau_1)}{8} \right]^{3/2}}, \quad (1)$$

$$\frac{3Ca}{\left[\left(\frac{w_1}{w_2} \right)^2 \left(\frac{\tau_1}{\tau_2} \right)^{5/2} + 1 \right] \left[\frac{w_2}{w_{in}} \right]} = \frac{\tau_2^{5/2}}{\left[\frac{7(1-\tau_2)}{8} \right]^{3/2}}, \quad (2)$$

where $\tau_1 = d_1/w_1$ and $\tau_2 = d_2/w_2$ as the smallest thickness of the thin film scaled with the width of the corresponding outlet channel. The capillary number (Ca) is

defined as

$$Ca = \frac{\mu U_{in}}{\gamma}, \quad (3)$$

with μ as the viscosity of the fluid of the continuous phase and γ as the surface tension between the two fluids. Equations (1) and (2) are major relations to calculate the smallest thickness of the thin film in the T junction with unequal channels. For the case of equal outlet channels ($w_1 = w_2 = w$) eqs. (1) and (2) will be reduced to the following:

$$\tau_1 = \tau_2 = \frac{d}{w} = \left(\frac{K}{2} \right)^{3/5} (6Ca)^{2/5} \Rightarrow K = \frac{7}{4}, \quad (4)$$

which is equal to the relation derived in ref. [13] for the smallest thickness in symmetric T junctions with assumption $1 - d/w \approx 1$. Using eqs. (1) and (2) one can calculate the smallest thickness of the thin film as a function of w_1/w_2 (see fig. 2) and as a function of capillary number (see fig. 3). As can be seen from fig. 2 by increasing w_1/w_2 the value d_1 (d_2) increases (decreases). This is because by increasing w_1/w_2 the volume of droplet entering the narrow (wide) branch increases (decreases). (However, the volume of droplet entering the wide branch is always larger than that of the narrow branch.)

For any capillary number there is a critical value for $w_1/w_2 = (w_1/w_2)_{critical}$ such that by selecting the value of w_1/w_2 less than $(w_1/w_2)_{critical}$, one obtains $d_1 = 0$ for the narrower branch and $d_2 \rightarrow \infty$ for the wider branch. The meaning of this situation is that no part of the droplet can enter the narrower branch. The critical values of w_1/w_2 linearly change with capillary number as depicted in fig. 2 with a long dashed line. For the case $w_1/w_2 = 1$, *i.e.*, a symmetric T junction we have $d_1/w_1 = d_2/w_2$. Also in fig. 2 the results of the simulation have been compared with analytical results for $Ca = 0.1$. As can be seen the numerical results are in a very close agreement with the analytical results.

According to fig. 3 at small capillary numbers with decreasing w_1/w_2 the changes of d_2/w_2 is much less than the changes of d_1/w_1 . Also for the case $w_1/w_2 = 1$ the curves d_1/w_1 and d_2/w_2 are coinciding at all the capillary numbers. The radius of curvature of the end parts of the droplet (r_1 and r_2 in fig. 1) can be obtained from the following relation:

$$r_1 = \frac{w_1 - d_1}{2} \Rightarrow \frac{r_1}{w_1} = \frac{1}{2} \left(1 - \frac{d_1}{w_1} \right); \quad (5)$$

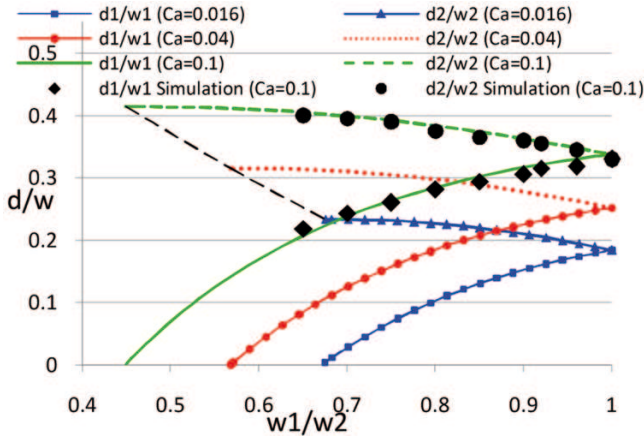


Fig. 2. The smallest thickness of the thin film as a function of w_1/w_2 (eqs. (1) and (2)). The critical values for w_1/w_2 for capillary numbers 0.016, 0.04 and 0.1 are 0.675, 0.568 and 0.429, respectively. $(w_1/w_2)_{\text{critical}}$ changes linearly *vs.* capillary number as is shown with a long-dashed line. Note that for $w_1/w_2 < 0.449$ the droplet does not break up and only enters into the wider channel.

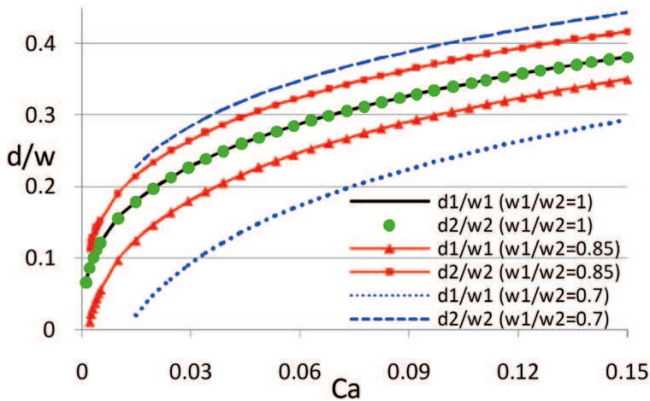


Fig. 3. The smallest thickness of the thin film as a function of capillary number (eqs. (1) and (2)). By increasing capillary number, d_2 increases more than d_1 .

if d_1/w_1 and d_2/w_2 are known the radius of curvature can be easily calculated.

4 Numerical algorithm

A Volume of Fluid (VOF)-based method [20] is used to study the two-phase flow system. Briefly the method solves the equations of momentum and continuity simultaneously for each of the fluids. To calculate the average viscosity, volume fraction of the phases ϕ have been used. ϕ in each cell is a value between 0 and 1 ($0 \leq \phi \leq 1$). The boundary is situated on the regions where ϕ is equal to 0.5. A piecewise linear interface reconstruction method is used to construct the boundary. For the surface tension a continuum surface force (CSF) model is also used [21,22]. The numerical procedure is checked to make sure that the results do not depend on the grid size and the time step size. Finally one node per $1 \mu\text{m}$ is used in the simulations

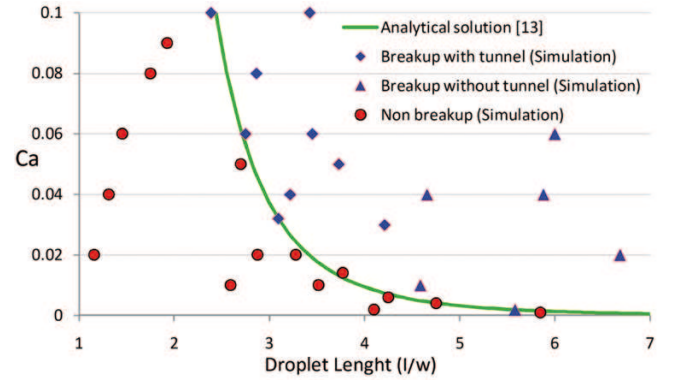


Fig. 4. The critical length as a function of capillary number for symmetric T junctions. The critical length is scaled with w . The breakup and non-breakup regions have been distinguished by the critical length curve (eq. (6)). Note that the capillary number is defined by $0.5U_{\text{in}}$. The triangle symbols indicate the occurrence of obstruction breakup and diamond symbols indicate the occurrence of breakup with tunnel. As can be seen when long droplets break up they fill the spaces of the outlets and prevent the formation of tunnel.

to determine the number of required nodes and also the time step size is considered to be 10^{-8} s. A QUICK routine is used for differencing the momentum equation and a SIMPLEC algorithm has been employed to couple the pressure and velocity. The convergence criterion is considered to be 0.0005.

5 Results and discussion

In this section we first validate the methods used in the study by considering symmetric T junctions. Then numerical results for asymmetric T junctions are presented. The production of non-uniform droplets in asymmetric T junctions can be via either breakup with tunnel or breakup without tunnel. In the first part we briefly consider breakup with tunnel and then we study breakup without tunnel or obstruction breakup in more detail.

5.1 Validation of the theory and the numerical simulations

In ref. [13] a relation for the critical length l , namely the extension of droplet just before the breakup (for better understanding this parameter note that in fig. 1 l is equal to $x_1^* + x_2^* + r_1 + r_2$) for the boundary region between regions of no breakup and breakup with tunnel, as a function of the capillary number and the width of the channel, was derived as

$$\frac{l}{w} = 1.3Ca^{-0.21}, \quad (6)$$

where w is the width of the channel. In order to check the reliability of the numerical result a numerical simulation was performed for a symmetric T junction and the results were compared with eq. (6). The results are depicted in fig. 4. Also in fig. 5 the analytical solution for a droplet

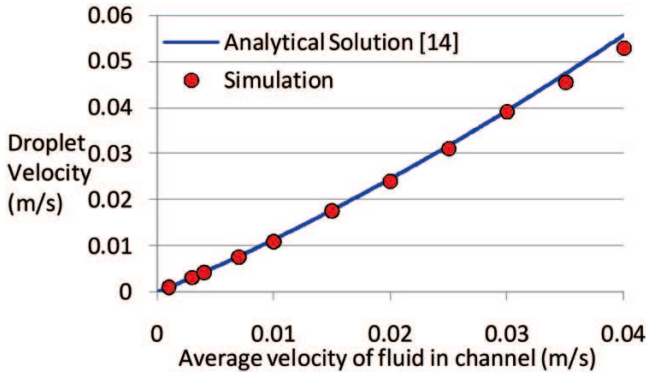


Fig. 5. Velocity of the droplet as a function of the average velocity in the pipe. There is a small difference between the numerical and analytical results for cases with average velocity above 0.03. This happens due to the fact that in the analytical solution it is assumed that the velocity is small.

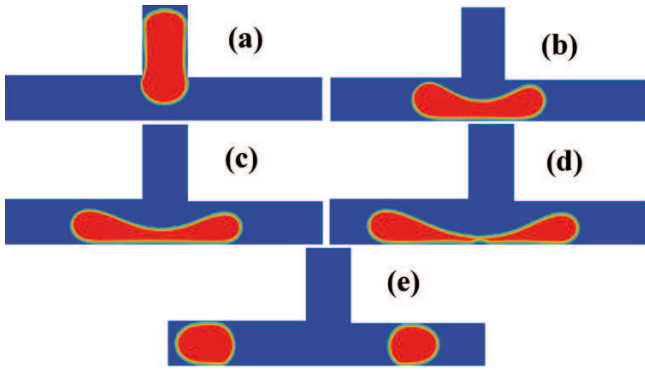


Fig. 6. Breakup of a droplet with tunnel for an asymmetric T junction. Ca is equal to 0.04 and the channel width ratio is 0.95. The dimensionless times ($U_{in}t/w_{in}$) are 2 (a), 4 (b), 4.8 (c), 6.48 (d), and 8 (e). U_{in} in dimensional form is equal to 0.16 m/s and the inlet channel has a width equal to 20 μm .

in a cylindrical pipe reported in ref. [14] has been compared with the results of the numerical simulation. Since the system in this case is axi-symmetric the simulation can be simplified to a 2-D simulation. In both the cases excellent agreement was obtained between the analytical and numerical results (see figs. 4 and 5).

5.2 Breakup with tunnel

Figure 6 shows a typical example of break with tunnel. In the simulation it is assumed that $w_2 = w_{in}$ and the length of the channels are equal. The channel width ratio is equal to 0.95 and Ca is equal to 0.04. For this case the velocity of the fluid in the film before the breakup is much larger than the velocity of the droplet in the narrower channel.

5.3 Breakup without tunnel

A typical result for the breakup without tunnel is shown in fig. 7. Similar to the case of breakup with tunnel, in the

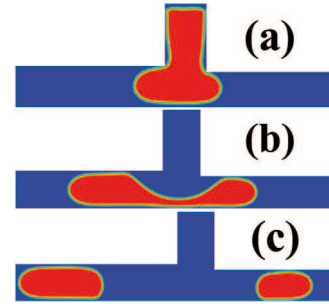


Fig. 7. The process of generating unequal-size droplets (obstruction regime). (a) The starting stage of the production, (b) the breakup process (c) the final stage. $w_1/w_2 = 0.85$, $Ca = 0.1$ and the volume ratio of the droplets is equal to 0.572.

simulation, it is assumed that $w_2 = w_{in}$ and the length of the channels are equal. The distribution of the pressure inside the system at the time of breakup is depicted in fig. 8 for this case. In fig. 9 the volume ratio of the droplet as a function of channel width ratio is also shown.

The results can be well described in terms of a power law function of w_1/w_2 . In each capillary number the vertical line shows a width ratio below which no droplet enters the narrower channel. Also based on fig. 9 by increasing the capillary number smaller droplets (in the narrower channel) can be produced. For example the minimum volume ratios of the droplets that can be produced for capillary numbers 0.016, 0.04 and 0.1 are 0.5363, 0.2206 and 0.1012, respectively. In the process of generating the droplets with a specific size, the droplets are transferred through several consecutive T junctions as depicted in fig. 10. By decreasing the distance between the droplets more droplets can enter the T junction in a period of time and consequently this will improve the efficiency of the system. The minimum distance between the droplets can be obtained from

$$X_{\min} = U_d \times t_{\text{breakup}}, \quad (7)$$

where X_{\min} and U_d represent the minimum distance between the droplets and velocity of the droplets in the inlet channel before reaching the junction, respectively. t_{breakup} is the breakup time of the droplets in the T junction (see fig. 11). Since U_d is an already known parameter, it can be stated that if t_{breakup} is reduced the distance between the droplets can also be reduced and as a result the rate of production will be increased. Figure 12 shows the time of the breakup in the system as a function of w_1/w_2 for several capillary numbers. According to the figure, the breakup time for any capillary number is independent of the channel width ratio and is almost constant but by increasing the capillary number the breakup time decreases. Therefore, the rate of production will be higher for larger values of the capillary number.

An examination of fig. 10 also reveals that there is an elbow after each T junction. Thus, by decreasing the distance between T junction and the elbow the performance of the system can be improved. However, the distance should be large enough such that a droplet enters

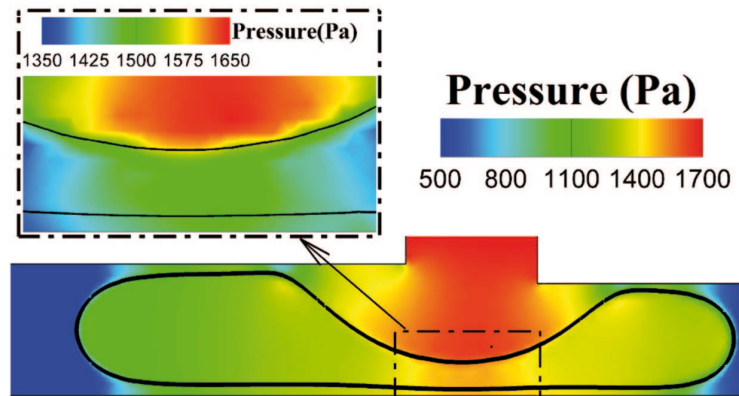


Fig. 8. The distribution of pressure for the system shown in part (b) of fig. 7. The inset shows the concentration of pressure in the region of breakup.

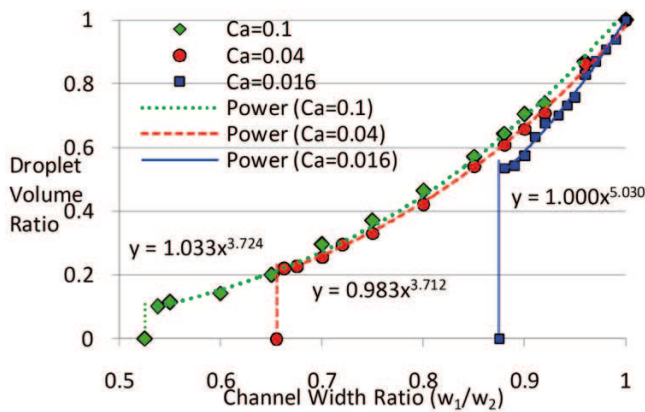


Fig. 9. The volume ratio of the droplets as a function of channel width ratio w_1/w_2 for the obstruction breakup regime. For $w_1/w_2 = 1$ (symmetric T junction) for all the capillary numbers the droplets entering the outlet channels have the same size. Also for creating a specific volume ratio as the capillary number decreases, the width ration should be chosen larger, namely, the T junction would be more similar to the symmetric T junction.

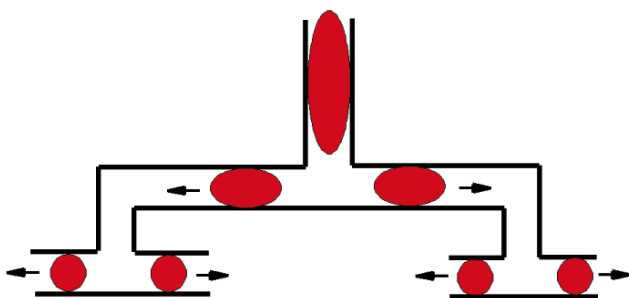


Fig. 10. Generation of equal-size droplets using consecutive symmetric T junctions (in order to see the actual system, see ref. [8]).

the junction only after breakup of the previous droplet. To handle the situation the length of the droplet at the time of the breakup that we call it breakup length of the droplet (see fig. 13) should be calculated first. For non-symmetric T junctions since the droplet is divided into

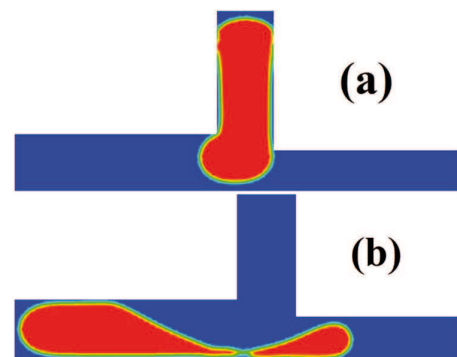


Fig. 11. The breakup time is the time between part (a) and part (b). In the shown case $w_1/w_2 = 0.71$ and $Ca = 0.04$.

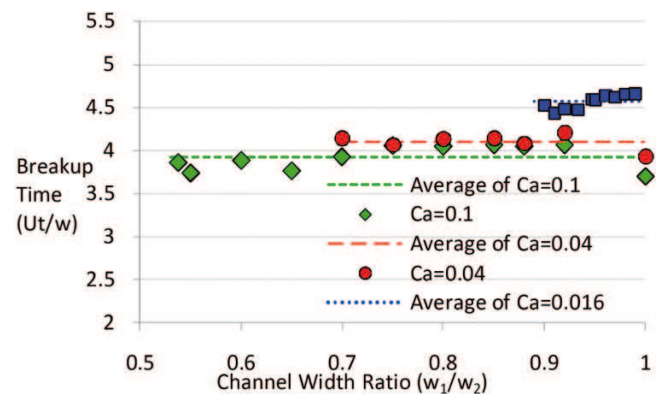


Fig. 12. The breakup time as a function of the channel width for the obstruction breakup regime. The breakup time t has been made dimensionless as Ut/w , where U is the velocity of the fluid in the inlet channel and w is the width of the channel. The average breakup times for $Ca = 0.016, 0.04$ and 0.1 are 4.569, 4.103 and 3.924, respectively.

two unequal parts, there are two breakup lengths. As a result, if the breakup length in one of the channels is minimized, the length of that channel will be optimized. In fig. 14 the droplet breakup length as a function of w_1/w_2 for some capillary numbers is shown. As the channel width decreases, since less (more) droplet volume enters the nar-

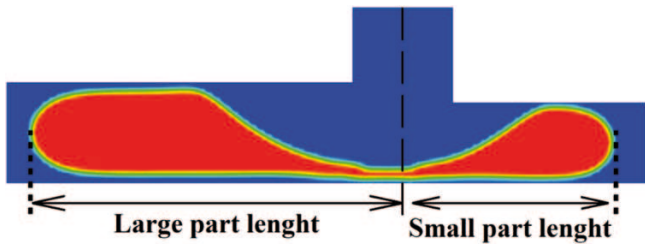


Fig. 13. The droplet breakup length for the channels. Note that because of the asymmetry associated with the system the breakup lengths are different and the breakup length is larger in the wider channel.

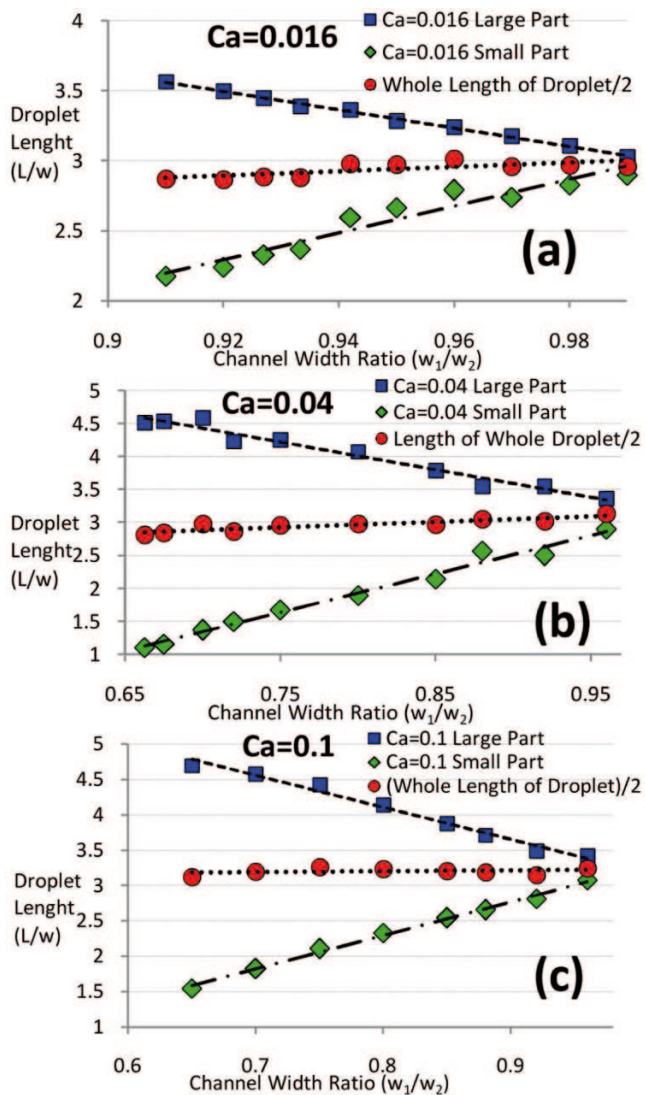


Fig. 14. The breakup length of the droplet as a function of the channel width ratio for the obstruction breakup regime. The breakup length has been scaled with the channel width. The breakup length is a linear function of the channel width for all the capillary numbers. As $w_1/w_2 \rightarrow 1$ (symmetric T junction) the produced droplets entering the channels have the same size, as expected, and the breakup lengths are equal.

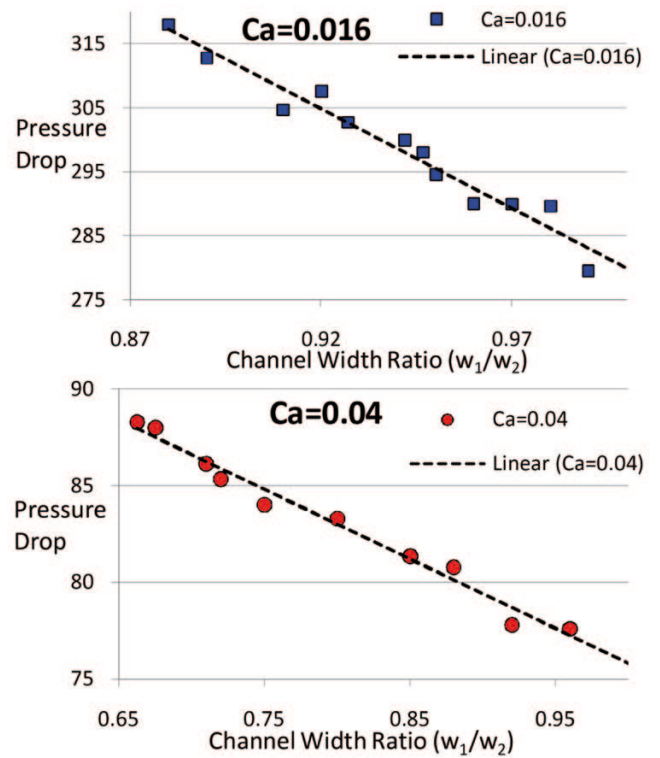


Fig. 15. The pressure drop as a function of channel width ratio for the obstruction breakup regime. The pressure drop has been made dimensionless as $\Delta p/\rho_e U_{in}^2$, where Δp is the pressure drop, ρ_e represents the density of the carrier liquid and U_{in} stands for the average velocity of the fluid transferring droplets in the inlet channel. In the figure the pressure drop is measured at the time of breakup.

rower (wider) channel, the breakup length of the smaller (larger) droplet will be smaller. As a result of reducing the breakup length in the narrower (wider) channel, the width ratio should decrease. In fluidic systems, the pressure drop is one of the main parameters that should be taken into account. Since the breakup process in symmetric and asymmetric T junctions is an unsteady process, the pressure drop takes different values during the process. For design purposes the maximum pressure drop should be considered. In fig. 15 the pressure drop of the system is shown at the time of breakup as a function of the channel width ratio. The numerical results indicate that this pressure drop can be approximately considered as the maximum pressure drop. By decreasing w_1/w_2 the pressure drop linearly increases. Also by increasing the capillary number the pressure drop increases such that at $w_1/w_2 = 0.88$ and capillary numbers equal to 0.016 and 0.04 the pressure drop is 1041.9 and 1654.5 Pa, respectively.

For an asymmetric T junction with unequal length outlets it is shown that droplets initially are driven towards the short outlet because of lower hydrodynamic resistance [23]. However, by increasing the number of droplets in the short branch, the hydrodynamic resistance increases and becomes larger than that of the long outlet. In this sit-

uation droplets at the T junction rather enter into the long outlet. By entering the droplets into the long outlet the hydrodynamic resistance in this branch increases as well. As a result, for such a system droplets are alternately distributed between the different outlets [23]. This behavior can be neglected for symmetric T junctions because the droplets are of the same size. For unequal length asymmetric T junctions this behavior can also be neglected provided that the hydrodynamic resistance in the short outlet always remains below that of the long outlet [8, 23]. On the other hand, as the outlet lengths become shorter this behavior diminishes because the number of droplets in the branches decreases and the hydraulic resistances do not change appreciably. Therefore, for an asymmetric T junction with unequal width (case of our study), since the length of the outlets is smaller than those of the outlets for an asymmetric T junction with unequal length, this behavior diminishes or can be completely neglected.

6 Conclusion

A VOF numerical algorithm was used to investigate a method to produce unequal-size droplets. An analytical theory in the limit of thin-film approximation was developed and by comparing the analytical and numerical results the validity of the numerical results were verified. The numerical results were also in agreement with already reported results for symmetric T junctions (the case $w_1/w_2 \rightarrow 1$). The effect of the width ratio on the volume ratio of the produced droplets were investigated and it was found that by increasing the capillary number smaller droplets can be produced. Two new parameters, *i.e.*, the breakup time and breakup length of the droplets, were introduced and the effect of the channel width ratio and capillary number on these parameters was studied. It was found that increasing the width ratio decreases the breakup length and consequently decreases the required length for the outlet channels. Also the pressure drop of the carrier fluid was investigated for different channel width ratios and capillary numbers and it was found that increasing the width ratio decreases the pressure drop. It was also found that by increasing the capillary number the breakup time decreases and the production speed increases but the pressure drop also increases. In order to compare the system with a T junction with different length of outlet channels, a series of simulations was performed. The results revealed that the breakup times for a volume ratios equal to 1.92 and 2.2 are about 13 and 17 percents smaller, respectively and the pressure drops (the maximum pressure drop occurs slightly before the complete breakup of the droplets) are also about 10% smaller for both the cases considered.

Appendix A.

Consider the geometry and the details shown in fig. 1. Suppose that the droplet is in a position that its velocity

is very small compared to the velocity of the carrier fluid (the results of the simulation confirm this). Applying the thin-film analysis for the space between the droplet and the top wall [14] for each of the channels the following relation for the thickness of the thin film $h(x)$ is obtained:

$$h_1^3 \frac{\partial^3 h_1}{\partial x_1^3} = 3 \frac{\mu u_1 w_1}{\gamma}, \quad h_2^3 \frac{\partial^3 h_2}{\partial x_2^3} = 3 \frac{\mu u_2 w_2}{\gamma}, \quad (\text{A.1})$$

where u_1 and u_2 are the average velocity of the carrier fluid in the small and large channels, respectively, and μ and γ are the viscosity of the carrier fluids and the surface tension between the carrier fluid and the fluid of the droplet, respectively. In the following the subscript 1 refers to the narrower branch. A similar analysis can be developed for the wider branch. Defining the dimensionless parameters η_1 and ζ_1 as

$$\eta_1 = \frac{h_1}{d_1}, \quad \zeta_1 = \frac{x_1}{d_1^{4/3} \left(\frac{3\mu u_1 w_1}{\gamma} \right)^{-1/3}}. \quad (\text{A.2})$$

Equation (A.1) will be reduced to the following dimensionless form:

$$\eta_1^3 \eta_1''' = 1. \quad (\text{A.3})$$

On the other hand, the radii of curvature of the region near $x_1 = x_1^*$, that are $1/(\partial^2 h_1/\partial x_1^2)$ and $(w_1 - d_1)/2$ before and after x_1^* , respectively, are almost equal. For calculating $\partial h_1/\partial x_1^2$ eq. (A.2) can be used:

$$\frac{dh_1}{dx_1} = \frac{d\eta_1}{d\zeta_1} \times d_1 = \frac{d\eta_1}{d\zeta_1} \frac{d\zeta_1}{dx_1} \times d_1 = \left(\frac{3\mu u_1 w_1}{\gamma d_1} \right)^{1/3} \frac{d\eta_1}{d\zeta_1} \quad (\text{A.4})$$

$$\frac{d^2 h_1}{dx_1^2} = \frac{d(dh_1/dx_1)}{dx_1} = \frac{(3\mu u_1 w_1)^{2/3}}{\gamma^{2/3} d_1^{5/3}} \times \frac{d^2 \eta_1}{d\zeta_1^2}, \quad (\text{A.5})$$

since $1/(\partial^2 h_1/\partial x_1^2) = (w_1 - d_1)/2$ eq. (A.4) will be

$$\frac{(3\mu u_1 w_1)^{2/3}}{\gamma^{2/3} d_1^{5/3}} \frac{d^2 \eta_1}{d\zeta_1^2} = \frac{2}{(w_1 - d_1)}; \quad (\text{A.6})$$

with definition $\tau_1 = d_1/w_1$ and simplification we have

$$\frac{\mu u_1}{\gamma} = \frac{2^{2/3}}{3 (d^2 \eta_1 / d\zeta_1^2)^{3/2}} \left[\frac{\tau_1^{5/3}}{1 - \tau_1} \right]^{3/2}. \quad (\text{A.7})$$

Equation (A.5) describes the relation between the thickness of the thin film (τ_1) with other parameters. As already mentioned this relation is related to a region near $x_1 = x_1^*$. So the value $d^2 \eta_1 / d\zeta_1^2$ should be calculated near $x_1 = x_1^*$. For this purpose eq. (A.3) should be solved with three boundary conditions. Two boundary conditions are $\eta_1' = 0$ and $(\eta_1)_{\min} = 1$ and for the third boundary condition an arbitrary value can be considered for $\eta_1'' = 0$. With numerical integration of eq. (A.3) with the boundary conditions and finding $\eta_1(\zeta_1)$, and calculating $d^2 \eta_1 / d\zeta_1^2$ near $\zeta_1 = \zeta_1^*$ it is observed that $d^2 \eta_1 / d\zeta_1^2$ near $\zeta_1 = \zeta_1^*$ is not dependent on $\eta_1''(0)$ (which is selected arbitrary) and is almost equal to 1.75.

Now the unknown u_1 in eq. (A.5) should be determined. The pressure drop in the thin film from $\Delta p_1 = \mu u_1 w_1 l_1 / d_1^3$ (where $l_1 \approx \sqrt{d_1 w_1 / 2}$) [13] and the pressure drop in the pipe (after droplet) from the Darcy-Weisbach equation $\Delta p_{\text{tube}} = \rho f L_1 u_1^2 / (2w_1)$ can be determined. Using a dimensional analysis it can be shown that the pressure drop in the pipe (after droplet) is negligible compared to the pressure drop in the thin film. Thus, $\Delta p_1 = \Delta p_{\text{film}} + \Delta p_{\text{tube}} \approx \Delta p_{\text{film}}$. The flow rate in the channels is divided such that the pressure drop is equal in the channels. In the relation for pressure drop in the thin film $l_1 \approx \sqrt{d_1 w_1 / 2}$, as a result we have $l_1 / l_2 = \sqrt{d_1 w_1 / d_2 w_2}$. Substituting this relation in $(\Delta p_{\text{film}})_1 = (\Delta p_{\text{film}})_2$ and upon simplification, we obtain

$$\frac{u_1}{u_2} = \frac{w_2^{3/2} d_1^{5/2}}{w_1^{3/2} d_2^{5/2}}, \quad (\text{A.8})$$

from the conservation of the mass we also have

$$Q_{\text{in}} = Q_1 + Q_2 \Rightarrow U_{\text{in}} w_{\text{in}} = u_1 w_1 + u_2 w_2, \quad (\text{A.9})$$

simultaneously solving eqs. (A.6) and (A.7) u_1 will be found as

$$u_1 = \frac{U_{\text{in}}}{\left[\left(\frac{w_1}{w_2} \right)^{1/2} \left(\frac{d_2}{d_1} \right)^{5/2} + 1 \right] \left[\frac{w_1}{w_{\text{in}}} \right]}. \quad (\text{A.10})$$

By substituting and using $d_2 / d_1 = (\tau_2 / \tau_1) \times (w_2 / w_1)$ and $d^2 \eta_1 / d\zeta_1^2 = 7/4$ one gets

$$\frac{3Ca}{\left[\left(\frac{w_1}{w_2} \right)^2 \left(\frac{\tau_2}{\tau_1} \right)^{5/2} + 1 \right] \left[\frac{w_1}{w_{\text{in}}} \right]} = \frac{\tau_1^{5/2}}{\left[\frac{7(1-\tau_1)}{8} \right]^{3/2}}, \quad (\text{A.11})$$

repeating a similar procedure for the second channel the following relation is obtained:

$$\frac{3Ca}{\left[\left(\frac{w_1}{w_2} \right)^2 \left(\frac{\tau_1}{\tau_2} \right)^{5/2} + 1 \right] \left[\frac{w_2}{w_{\text{in}}} \right]} = \frac{\tau_2^{5/2}}{\left[\frac{7(1-\tau_2)}{8} \right]^{3/2}}. \quad (\text{A.12})$$

References

1. A.M. Ganan-Calvo, Phys. Rev. Lett. **80**, 28 (1998).
2. A.M. Burns, B.N. Johnson, S.N. Brahmaandra, K. Handique, J.R. Webster, M. Krishnan, T.S. Sammarco, P.M. Man, D. Jones, D. Heldsinger, C.H. Mastrangelo, D.T. Burke, Science **282**, 484 (1998).
3. T. Thorsen, R.W. Roberts, F.H. Arnold, S.R. Quake, Phys. Rev. Lett. **86**, 4163 (2001).
4. S. Sugiura, M. Nakajima, S. Iwamoto, M. Seki, Langmuir **17**, 5562 (2001).
5. J. Tice, H. Song, A. Lyon, R. Ismagilov, Langmuir **19**, 9127 (2003).
6. S.L. Anna, N. Bontoux, H.A. Stone, Appl. Phys. Lett. **82**, 364 (2003).
7. V. Cristini, Y. Tan, Lab Chip **4**, 257 (2004).
8. D.R. Link, S.L. Anna, D.A. Weitz, H.A. Stone, Phys. Rev. Lett. **92**, 054503 (2004).
9. M. Prakash, N. Gershenfeld, Science **315**, 832 (2007).
10. O. Sybulski, P. Garstecki, Lab Chip **10**, 484 (2010).
11. R. Gupta, D.F. Fletcher, B.S. Haynes, Chem. Eng. Sci. **64**, 2941 (2009).
12. Y. Yamasaki, M. Goto, A. Kariyasaki, S. Morooka, Y. Yamaguchi, M. Miyazaki, H. Maeda, Korean J. Chem. Eng. **26**, 1759 (2009).
13. A.M. Leshansky, L.M. Pismen, Phys. Fluids **21**, 023303 (2009).
14. F.B. Bretherton, J. Fluid Mech. **10**, 166 (1961).
15. E. Um, S.G. Lee, J.K. Park, Appl. Phys. Lett. **97**, 153703 (2010).
16. K.L. Lao, J.H. Wang, G.B. Lee, Microfluid Nanofluid **7**, 709 (2009).
17. W. Li, E.W.K. Young, M. Seo, Z. Nie Z, P. Garstecki, C.A. Simmons, E. Kumacheva, Soft Matter **4**, 258 (2008).
18. M.-C. Jullien, M.-J. Tsang Mui Ching, C. Cohen, L. Menetrier, P. Tabeling, Phys. Fluids **21**, 072001 (2009).
19. S. Afkhami, A.M. Leshansky, Y. Renardy, Phys. Fluids **23**, 022002 (2011).
20. B. Lafaurie, C. Nardone, R. Scardovelli, S. Zaleski, G. Zanetti, J. Comput. Phys. **113**, 134 (1994).
21. J.U. Brackbill, D.B. Kothe, C. Zemach, J. Comp. Phys. **100**, 335 (1992).
22. Y. Renardy, Rheol. Acta **46**, 521 (2007).
23. W. Engl, M. Roche, A. Colin, P. Panizza, Phys. Rev. Lett. **95**, 208304 (2005).